*Malaysian Journal of Chemistry, 2026, Vol. 28(2), 142-152*

# Synthesis and Optimization of a Molecularly Imprinted Polymer for the Adsorption of Fluorene

**Muhammad Yudhistira Azis, Muhammad Rahadian Nur Jabbar Rahman, Ahmad Mukhlasul Amri, Muhammad Ali Zulfikar, Aria Pinandita and Andi Budi Bakti***

Analytical Chemistry Research Division, Department of Chemistry, Faculty of Science and Mathematics, Bandung Institute of Technology, Bandung, 40132 Indonesia

*Corresponding author (email: andibudi055@gmail.com)

Fluorene, a low-molecular-weight PAH, poses environmental hazards due to its persistence, toxicity, mutagenicity, and teratogenicity. Molecularly imprinted polymers (MIPs) are widely used for the adsorption of organic pollutants, offering high selectivity, stability, and cost-effectiveness. This study aimed to synthesize, characterize, and evaluate the fluorene adsorption performance of an MIP, including isotherm, kinetics, and thermodynamic analyses. The MIP was synthesized using a 1:4:20 mole ratio of fluorene, divinylbenzene (DVB), and ethylene glycol dimethacrylate (EGDMA) in acetonitrile via bulk polymerization. FTIR spectra confirmed the characteristic C=O stretching vibration of EGDMA (1735 $cm^{-1}$) and the benzene ring skeletal vibration of DVB (1628 $cm^{-1}$), while SEM analysis revealed uniform microspheres (~3510 nm). Optimal adsorption occurred at 15 min, with 20 mg MIP and an initial fluorene concentration of 1200 ppb. Adsorption followed the Langmuir isotherm and pseudo-second-order kinetics, with the MIP achieving a maximum adsorption capacity of 13.5 mg/g. Thermodynamic analysis indicated an endothermic reaction ($\Delta H^\circ > 0$) and spontaneous adsorption ($\Delta G^\circ < 0$).

**Keywords**: Molecularly Imprinted Polymers, adsorption, divinylbenzene, fluorene

*Received: November 2025; Accepted: January 2026*

Polycyclic aromatic hydrocarbons (PAHs) are a class of organic compounds with multiple aromatic rings, which are categorized by their rings into low-molecular-weight (LMW) PAHs (2–3 aromatic rings) or high-molecular-weight (HMW) PAHs (4 or more aromatic rings) [1]. Fluorene, an LMW PAH, is a pollutant of significant concern due to its toxicity, mutagenicity, and teratogenicity, which pose risks to ecosystems and human health [2, 3]. Its stability and persistence in the environment further exacerbate its potential for harm, necessitating effective remediation strategies [4].

Various methods have been explored to remove fluorene from environmental matrices, including biodegradation, photolysis, and chemical oxidation [5]. Biodegradation relies on microorganisms to break down fluorene. However, it is a time-intensive process, and its efficiency decreases as the pollutant concentration declines [6]. Photolysis, which uses light energy to disrupt molecular structures, is limited by fluorene's stable aromatic configuration, which makes it resistant to this approach [7]. Chemical oxidation, which can lead to the formation of new intermediate pollutants, can sometimes be as toxic, or even more toxic, than fluorene [8]. Among the available methods, adsorption has emerged as a promising alternative for removing hydrophobic and persistent organic pollutants such as fluorene.

Adsorption involves the adhesion of molecules onto a solid surface, and is favoured for its simplicity and efficiency. Common adsorbent materials such as activated carbon and biochar have been widely studied. Activated carbon is particularly effective due to its large surface area and versatile forms, including powder and granules. However, its single-use nature and cost limitations reduce its long-term applicability [9]. Biochar, a sustainable and cost-effective material, has shown potential for fluorene removal. Despite its advantages, biochar's lack of selectivity in adsorbing specific molecules limits its performance in complex systems [10].

To address these limitations, molecularly imprinted polymers (MIPs) have been developed as advanced adsorbents with high selectivity. MIPs are synthesized using template molecules that create specific cavities within the polymer, matching the target molecule's shape, size, and functional groups [11, 12]. This design enables MIPs to selectively adsorb target molecules even in the presence of structurally similar compounds [13]. In addition to their selectivity, MIPs are reusable and robust, making them an attractive option for environmental remediation [14].

In this study, an MIP was synthesized using divinylbenzene (DVB) as the functional monomer,

ethylene glycol dimethacrylate (EGDMA) as the cross-linker, benzoyl peroxide (BPO) as the initiator, and acetonitrile as the solvent. Fluorene was used as the template molecule. Although it is toxic, using fluorene as a direct template for the MIP offers higher specificity compared to using a dummy template, because the imprinted cavities are perfectly complementary to the target molecule. The performance of the MIP was evaluated through adsorption studies, including contact time, MIP mass, initial fluorene concentration, and temperature.

This research highlights the potential of MIPs as a selective adsorbent by addressing the limitations of traditional adsorbents for fluorene removal, such as non-selectivity and single-use constraints. Traditional adsorbents rely primarily on non-specific physical interactions, leading to competitive adsorption and reduced performance in complex environmental matrices where fluorene coexists with other PAHs.

## EXPERIMENTAL

### Materials and Instrumentations

The materials used were fluorene (Sigma Aldrich), phenanthrene (Sigma Aldrich), divinylbenzene (Sigma Aldrich), ethylene glycol dimethacrylate (Merck, ≥98%), benzoyl peroxide (Merck, 75%), nitrogen gas, acetonitrile (Merck), and deionized water.

The instruments used were a Fourier Transform Infrared (FTIR) spectrophotometer (Prestige-21, Shimadzu-Japan), a Scanning Electron Microscope (SEM) (JEOL JSM-6510), and a High-Performance Liquid Chromatograph (HPLC) (Agilent 1260 Infinity, 1260 DAD VL). The HPLC system was equipped with a C-18 reversed-phase column (Fortis UniverSil, 5 µm particle size, 250 mm × 4.6 mm). The mobile phase consisted of acetonitrile and water (70:30, *v*/*v*), delivered at a flow rate of 1.0 mL/min, while detection was carried out at 254 nm.

### Synthesis of the Molecularly Imprinted Polymer

In the traditional preparation method, the molar ratio of template molecule and functional monomer to crosslinker was 1:4:20 [15]. So, the MIP was synthesized using a mole ratio of 1:4:20 for fluorene (template): DVB (functional monomer): EGDMA (crosslinker). The synthesis began by dissolving 166.2 mg of fluorene, the template molecule, in 50 mL of acetonitrile in a sealed container. Subsequently, 559.9 µL of DVB was added to the solution, followed by 3760 µL of EGDMA. The resulting mixture was stirred for 5 min using a mechanical shaker to ensure homogeneity. The solution was then purged with nitrogen gas for 15 min to remove oxygen, which could interfere with the polymerization. Then, 100 mg of BPO was added as the radical initiator, and nitrogen gas was passed through the mixture for an additional 5 min. The mixture was heated in an oil bath pre-set to 50 °C. The temperature was gradually increased to 70 °C and maintained for 30 min to facilitate polymerization. The resulting polymer mixture was cooled to room temperature. As a control, a non-imprinted polymer (NIP) was synthesized under identical conditions, but without including the template molecule.

### Release of Mold Molecule

A total of 1 g of the MIP was placed in a 100 mL Erlenmeyer flask, and 25 mL of acetonitrile was added as the solvent. The mixture was stirred using a shaker at 125 rpm for 30 min. After the stirring period, the solution was separated from the polymer using filtration or decantation. The polymer obtained was then added to another 25 mL of fresh acetonitrile, and stirred as before. This step was repeated for 15 cycles to ensure optimal release of the mould molecules from the polymer cavity. The release of the mould molecules (leaching) was monitored by HPLC, which detected fluorene peaks (254 nm) in the solution. Leaching was considered complete when fluorene peaks were no longer detected in the solution, indicating the full release of the mould molecules. This process yielded a leached MIP product for further evaluation.

### Characterization Methods

FT-IR analysis using the KBr pellet method identified functional groups over the wavenumber range of 4000─450 $cm^{-1}$. The SEM was used to observe the morphology of materials.

### Batch Adsorption Experiment

The performance of the MIP in terms of fluorene adsorption was evaluated by optimizing contact time (4-120 min), MIP mass (10-35 mg), initial fluorene concentration (600-1400 ppb), and temperature (25-60 °C). Isotherm studies were conducted to measure the adsorption capacity of the MIP at optimum conditions for each pre-optimized variable, with fluorene concentrations ranging from 600 to 1800 ppb.

The Langmuir, Freundlich, and Temkin isotherm models are widely employed to describe adsorption processes based on the nature of the adsorbent surface and the interaction energies involved. The Langmuir isotherm, represented by Equation (1), characterizes adsorption on a homogeneous surface, assuming monolayer adsorption with a finite number of active sites, utilizing parameters such as maximum adsorption capacity ($q_m$), Langmuir constant ($K_L$), equilibrium concentration ($C_e$), and equilibrium adsorption capacity ($q_e$) [16]. Conversely, the Freundlich isotherm, described by Equation (2), explains adsorption on heterogeneous surfaces,

involving parameters such as adsorption intensity (n) and the Freundlich constant ($K_f$) [17], [18]. The Temkin isotherm, as per Equation (3), considers the decline in adsorption energy as surface coverage increases, incorporating parameters like equilibrium binding constant ($K_T$), heat of adsorption constant (b), ideal gas constant (R), and temperature (T), thus providing a comprehensive framework for understanding adsorption phenomena [17], [18].

$$\frac{C_e}{q_e} = \frac{1}{q_m K_L} + \frac{C_e}{q_m} \quad (1)$$

$$\log q_e = \log K_f + \frac{1}{n}\log C_e \quad (2)$$

$$q_e = \frac{RT}{b}\ln K_T + \frac{RT}{b}\ln C_e \quad (3)$$

In the adsorption kinetics study, the adsorption of fluorene using the MIP was carried out under optimal conditions, and the residual concentration in the solution was measured by HPLC at specified time intervals. The thermodynamic study of adsorption was carried out by contacting the MIP under three temperature conditions, with the same adsorbate concentration, and then measuring the adsorbed solution using HPLC. The adsorption capacity was calculated from the fluorene concentration in the supernatant using Equations (4) and (5).

$$q_e = \frac{(C_i - C_e)v}{m} \quad (4)$$

$$\%adsorption = \frac{(C_i - C_e)}{C_i}\ x\ 100\% \quad (5)$$

where $q_e$ is the adsorption capacity (mg/g), $C_i$ is the initial concentration of fluorene (mg/L), $C_e$ is the equilibrium concentration of fluorene (mg/L), V is the volume of solution (L) and m is the MIP mass (g).

## RESULTS AND DISCUSSION

### Synthesis of MIP

The molecularly imprinted polymer (MIP) was synthesized using a mole ratio of 1:4:20, with 1 mole of fluorene as template, 4 moles of DVB as the functional monomer, and 20 moles of EGDMA. Fluorene is a PAH composed of three cyclic structures, including two aromatic rings, and is classified as an LMW compound. The synthesized MIP prepared with acetonitrile as the porogen solvent yielded 3.7822 g of a white solid, corresponding to an 81.28 % yield, calculated based on the experimental product mass.

### Characterization

The FTIR characterization results (Figure 1 and Table 1) revealed distinct absorption peaks at specific wavenumbers. The characteristic C=O stretching vibration of EGDMA was observed at 1735 $cm^{-1}$. The benzene ring skeletal vibration of DVB was observed at 1628 $cm^{-1}$, while the methylene (–$CH_2$–) stretching vibrations of EGDMA and DVB appeared at 2965 $cm^{-1}$ [19]. The results indicate that the MIP was successfully synthesised. Characterization of the non-imprinted polymer (NIP), MIP, and leached MIP revealed consistent spectral patterns, indicating structural similarities.

However, definitive confirmation of complete fluorene removal may not be possible based solely on infrared analysis, due to the overlap of characteristic aromatic C=C stretching peaks. Therefore, to complement the FTIR results and provide strong verification of fluorene elimination from the MIP, thermal analysis using thermogravimetric analysis (TGA) and derivative thermogravimetry (DTG) should be conducted. This approach enables the observation of characteristic thermal degradation patterns associated with the presence or absence of fluorene [20].

**Table 1.** Peak assignments for the infrared spectrum of MIP.

| Bond vibration | Wavenumber ($cm^{-1}$) |
|---|---|
| C-H stretching (alkanes) | 2965 |
| C=O stretching | 1735 |
| C=C stretching (alkenes) | 1628 |
| C=C stretching (aromatic) | 1464–1148 |

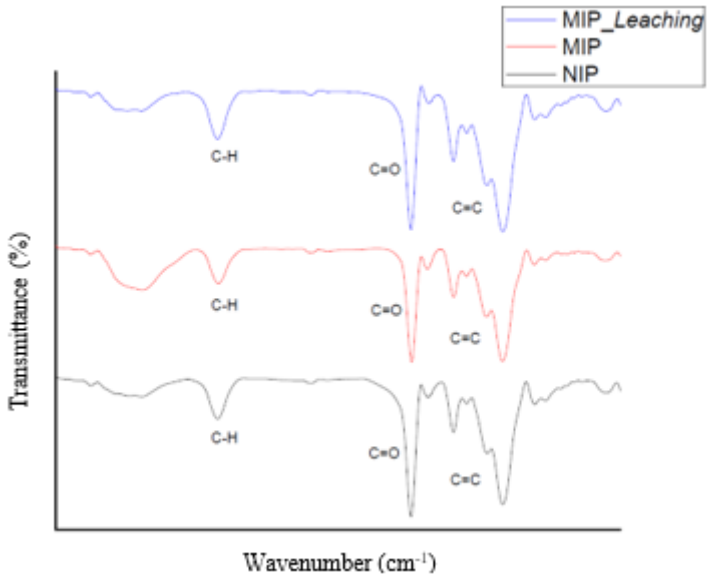


**Figure 1.** IR spectra of NIP, MIP and leached MIP.

The MIP and NIP were characterized using scanning electron microscopy (SEM). SEM analysis was conducted at an accelerating voltage of 10 kV with magnifications of 2,500x (left) and 20,000x (right). The NIP and MIP images are shown in Figure 2. The results demonstrate apparent differences in the surface morphologies of NIP and MIP.

A magnification of 2,500× was selected to observe the uniformity of the synthesized polymer surfaces, while 20,000× magnification provided detailed insights into particle shapes and sizes. The NIP sample exhibited irregular surfaces, with poorly defined and unmeasurable particle shapes. In contrast, the MIP sample displayed well-formed, spherical surfaces, enabling precise particle measurement. The template molecule (fluorene) served as a structure-directing agent, influencing and directing the formation of specific topological structures in the material. Therefore, aggregation was more pronounced in the NIP, where the absence of the template led to less controlled structural organization [21].

Furthermore, the MIP retained its spherical morphology after leaching, indicating that the leaching process did not damage the polymer structure. The resulting MIP morphology showed well-defined microspheres, consistent with a report by Krupadam [22].

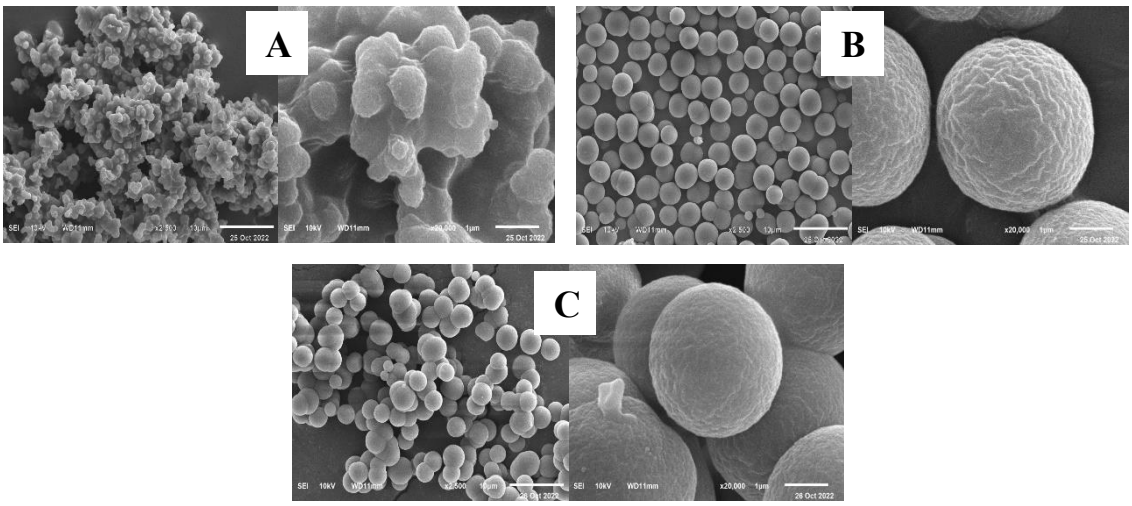


**Figure 2.** SEM images of (A) NIP, (B) MIP and (C) MIP after leaching.

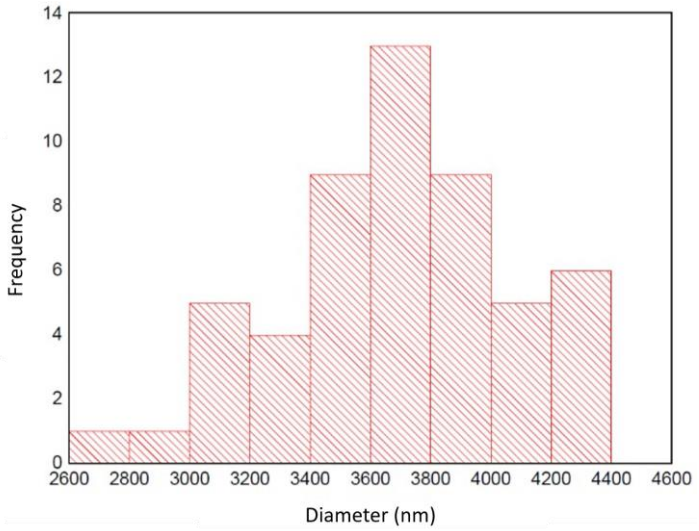


**Figure 3.** Particle size histogram.

The diameter of the MIP particles were measured before and after leaching, and were found to be larger than those reported in the literature, which were around 1038─2702 nm [23]. Our study found the most common particle size range was 3600-3800 nm, with an average diameter of 3510 nm. The histogram distribution of particle size is shown in Figure 3. Polymer morphology, particle size, and template–monomer interactions are influenced by the properties of the monomers, cross-linker, and solvent [24].

**Adsorption Activity Studies**

As shown in Figure 4(A), the amount of fluorene adsorbed increased with contact time, indicating progressive saturation of the MIP's active sites. Contact time is a critical parameter in adsorption studies, representing the time required for an adsorbent to achieve maximum pollutant adsorption until equilibrium is reached [25]. For the MIP, optimal adsorption was achieved at 15 min, as indicated by the plateau in the adsorption curve, reflecting efficient and selective binding to the imprinted sites. In contrast, the NIP reached equilibrium at 25 min, suggesting adsorption driven by non-specific interactions. The shorter equilibrium time and higher adsorption efficiency of the MIP compared to the NIP demonstrates the advantages of molecular imprinting in creating specific binding sites for target molecules.

Figure 4(B) shows a decreasing trend in adsorption capacity with increasing MIP mass, while the adsorption percentage (%adsorption) increased. This outcome was attributed to the fixed volume (200 mL) and concentration (1000 ppb) of fluorene solution used in the experiments, irrespective of the MIP mass.

At higher MIP masses, such as 35 mg, the adsorption capacity per unit mass decreased due to increased competition among active sites within the MIP particles. This competition limits the effective use of available binding sites, reducing adsorption capacity. On the other hand, the %adsorption continued to rise as the overall fluorene concentration in the solution diminished with increasing MIP mass. The optimal MIP mass was identified as 20 mg, at which the adsorption capacity and %adsorption reached a balanced state, maximizing the adsorption process efficiency.

The results in Figure 4(C) show a clear trend: adsorption capacity increased with fluorene concentration, indicating progressive occupation of the MIP's active sites. At an initial fluorene concentration of 1200 ppb (Ceq 200 ppb), the adsorption capacity approached near-optimal levels, as evidenced by the plateau in the adsorption curve. This plateau suggests that the MIP's active sites were nearing saturation, and further increases in fluorene concentration yielded minimal changes in adsorption capacity. The observation that the adsorption capacity levelled off at higher concentrations highlights the adsorbent's finite number of active sites and its maximum adsorption potential under the given conditions.

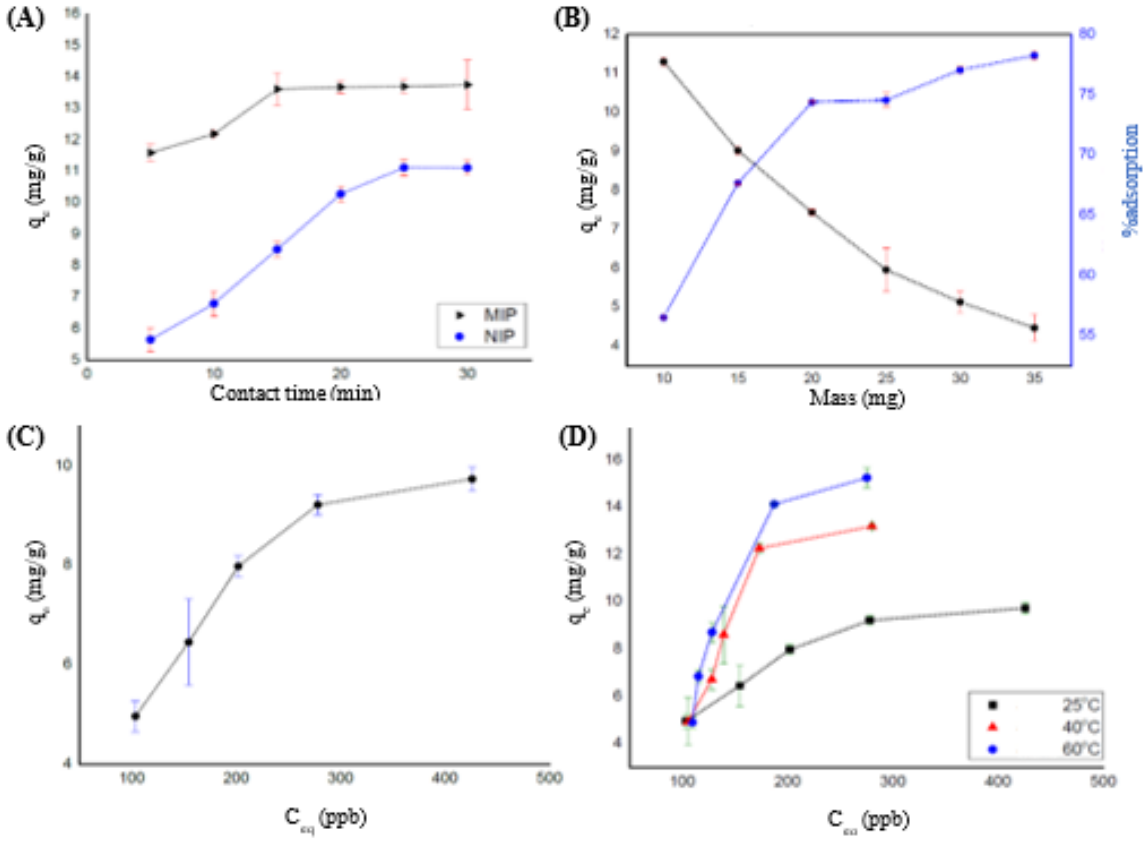


**Figure 4.** Effects of (a) contact time, (b) MIP mass, (c) initial fluorene concentration, (d) temperature, on fluorene adsorption.

Temperature significantly influences the adsorption process. An increase in temperature generally increases kinetic energy, accelerating collisions between the MIP and fluorene molecules, thereby improving adsorption. This enhanced adsorption leads to a higher adsorption rate and increased adsorption capacity [17].

The adsorption experiments were conducted at 25 °C, 40 °C, and 60 °C. These temperatures were selected because water, the solvent, has a boiling point of 100 °C. Temperatures above 60 °C were avoided to prevent approaching the solvent's boiling point, which could compromise the system's stability and the adsorption process. As shown in Figure 4(D), adsorption capacity increased with temperature. This trend suggests that the adsorption process was endothermic, where higher temperatures enhance the mobility of the fluorene molecules and improve the interaction between the MIP and fluorene.

Adsorption isotherms are essential for understanding the mechanisms and interactions between the adsorbent and adsorbate during adsorption. In this study, the three isotherm models used were the Langmuir, Freundlich, and Temkin models (Figure 5).

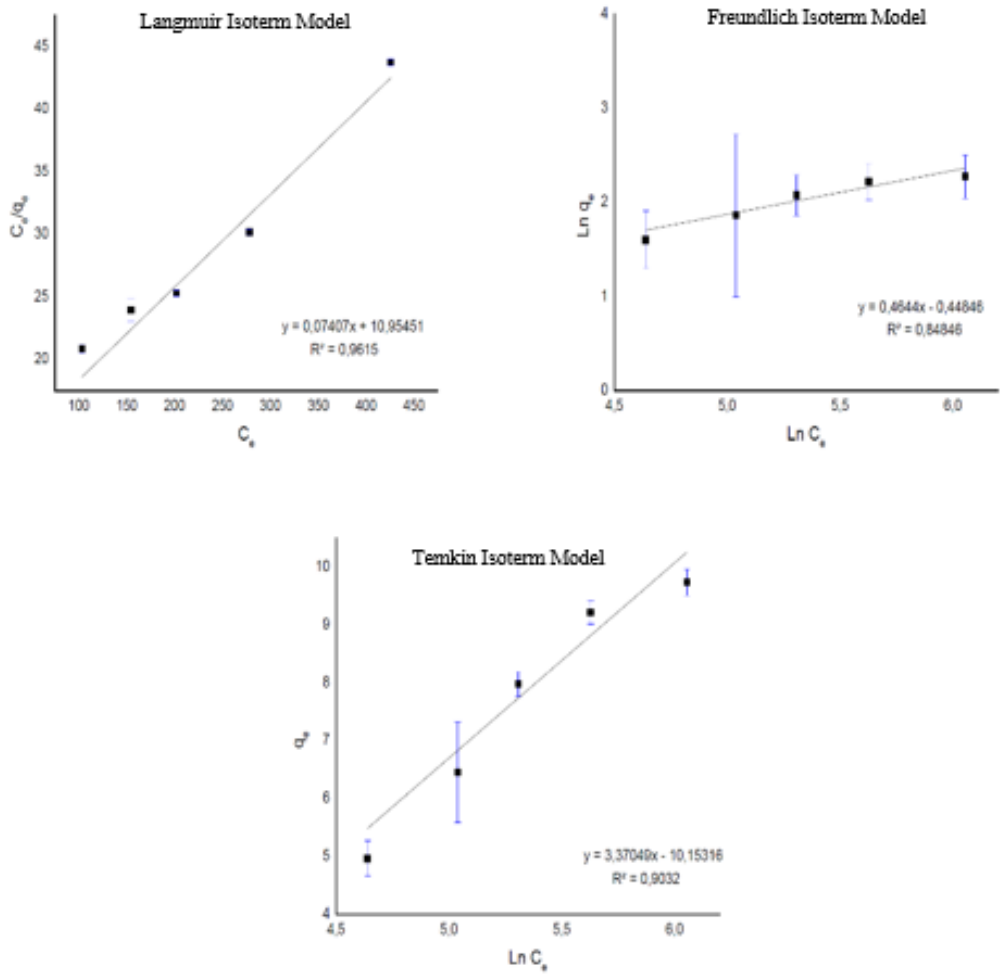


**Figure 5.** Isotherm adsorption model.

**Table 2.** Adsorption Isotherm Parameters.

| Langmuir | | | Freundlich | | | Temkin | | |
|---|---|---|---|---|---|---|---|---|
| $q_m$ (mg/g) | $K_L$ (L/mg) | $R^2$ | $K_F$ (L/mg)$^{1/n}$ | N | $R^2$ | B (J/mol) | $K_T$ (L/g) | $R^2$ |
| 13.5007 | 0.0067 | 0.961 | 0.6398 | 2.1533 | 0.848 | 735.4476 | 0.0492 | 0.903 |

From Table 2, the Langmuir model had the highest $R^2$ value, indicating the highest degree of linearity among the models. This result suggests that the adsorption process followed the Langmuir isotherm model. The Langmuir isotherm describes adsorption occurring on a homogeneous monolayer surface, where each adsorption site has uniform energy [26]. Once a monolayer is formed, the MIP surface becomes saturated, and no further adsorption can occur. This characteristic aligns with the experimental data, supporting the assumption of monolayer adsorption.

The maximum adsorption capacity ($q_m$) of the MIP synthesized using DVB and EGDMA toward fluorene was 13.5007 mg $g^{-1}$. This is relatively higher than the reported values of some MIPs for PAHs prepared with different functional monomers and crosslinkers, particularly those based on MAA (see Table 3). Variations in adsorption capacities across studies can be attributed to differences in polymer composition and target PAH structures.

**Kinetic Adsorption Study**

The reaction kinetics were determined by plotting time against $\ln(q_e - q_t)$ for pseudo-first-order reactions, and time against $t/q_t$ for pseudo-second-order reactions. As shown in Figure 6 (for NIP), the $R^2$ value for the pseudo-second-order model was closer to 1 (0.96794)

compared to the pseudo-first-order model, indicating higher linearity. Similarly, for MIP (Figure 7), the $R^2$ value was 0.99755, further confirming that the adsorption kinetics for fluorene followed the pseudo-second-order model.

The pseudo-second-order kinetic model is commonly associated with chemisorption processes, which are governed by strong chemical interactions such as covalent bonding or ion exchange. From a theoretical perspective, this model implies that the adsorption process involves multiple active sites on the adsorbent surface [31]. The rate constant ($k_2$) was calculated to be 0.02965 $g \cdot mg^{-1} \cdot min^{-1}$ for MIP and 0.00620 $g \cdot mg^{-1} \cdot min^{-1}$ for NIP. These values further highlight the faster adsorption kinetics of MIP compared to NIP, consistent with its design and higher specificity for fluorene.

**Table 3.** Adsorption capacities of MIPs for various PAHs.

| Functional Monomer | Crosslinker | Target PAHs | Adsorption Capacity (mg/g) | Reference |
|---|---|---|---|---|
| MAA | EGDMA | BaP, Pyr, Cry | 0.0759; 0.0069; 0.0071 | [27] |
| MAA | TMPTMA | BaP | 0.0078 | [28] |
| MAA | EGDMA | BaA, BaP, BbF, Chry, DaP, IP | 0.116; 0.111; 0.118; 0.115; 0.110; 0.117 | [29] |
| - | NOBE | Pyr | 35 | [30] |
| DVB | EGDMA | Fl | 13.5 | This work |

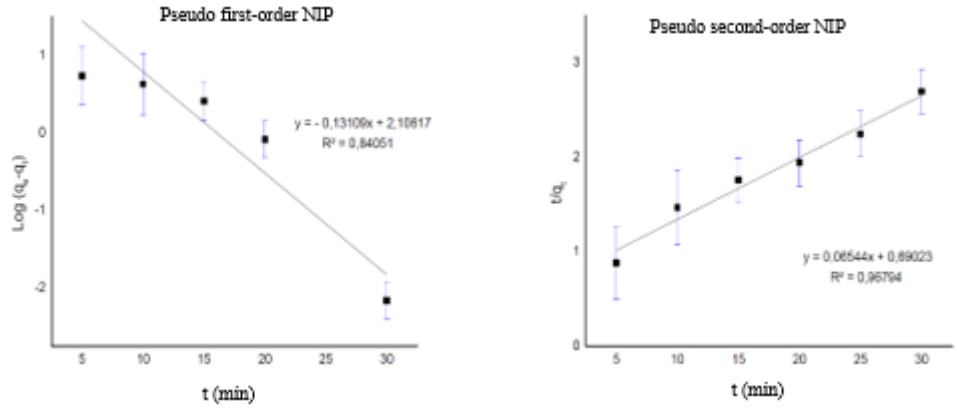


**Figure 6.** Pseudo first-order (left) and pseudo second-order (right) NIP reaction kinetics.

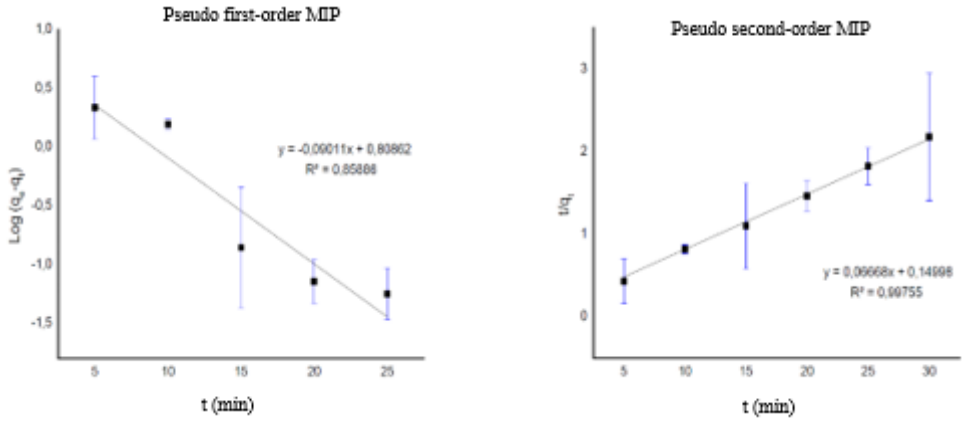


**Figure 7.** Pseudo first-order (left) and pseudo second-order (right) MIP reaction kinetics.

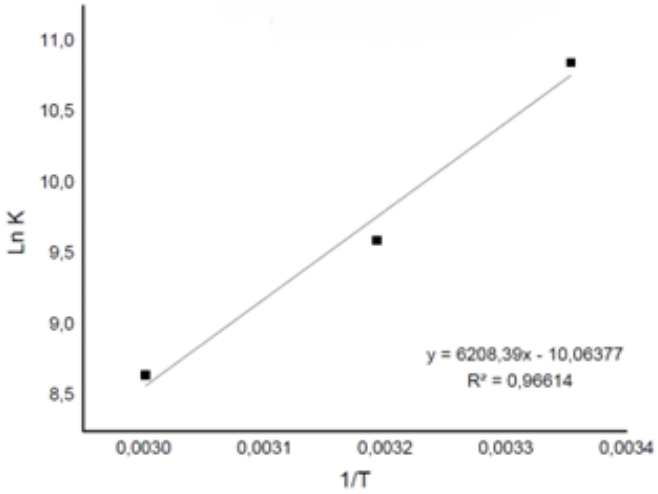


**Figure 8.** Plot of 1/T against Ln K.

**Table 4.** Adsorption Thermodynamics Parameters.

| Temperature (°C) | $\Delta G°$ (kcal.mol$^{-1}$) | $\Delta H°$ (kcal.mol$^{-1}$) | $\Delta S°$ (cal.mol$^{-1}$K$^{-1}$) |
|---|---|---|---|
| 25 | -9.2506 | | |
| 40 | -9.88656 | 3.7134 | 43.4629 |
| 60 | -10.7714 | | |

**Thermodynamic Adsorption Study**

Thermodynamic studies were conducted using temperature-dependent data to evaluate the adsorption characteristics of fluorene. From the graph in Figure 8, equations were derived to calculate the thermodynamic parameters ΔG°, ΔS°, and ΔH°.

The Gibbs free energy change (ΔG°) indicates the spontaneity of the reaction: a negative value reflects a spontaneous process. The entropy change (ΔS°) represents the system's disorder, where a positive value indicates increased disorder. Enthalpy change (ΔH°) describes the energy involved in adsorption; a positive ΔH∘ indicates heat absorption, indicating an endothermic reaction. The calculated thermodynamics parameters for this study are presented in Table 4, providing insights into the energy dynamics, spontaneity, and entropy changes associated with the adsorption process.

Ideally, adsorption processes in which an increase in temperature corresponds to an increase in adsorption capacity are endothermic, as higher temperatures favour adsorption due to heat absorption. The result is consistent with the calculations in this study which gave a positive ΔH∘ value, indicating that the reaction was endothermic and that the adsorption process absorbed heat.

## CONCLUSION

This study successfully synthesized and characterized a fluorene-based molecularly imprinted polymer (MIP) with a focus on adsorption performance. The MIP exhibited a maximum adsorption capacity of 13.5 mg/g. Structural characterization using FTIR confirmed the presence of functional groups, and SEM analysis revealed uniform microsphere morphology (~3510 nm). The adsorption process followed the Langmuir isotherm, indicating monolayer adsorption, and adhered to pseudo-second-order kinetics. Thermodynamic parameters suggested an endothermic ($\Delta H° > 0$) and spontaneous process ($\Delta G° < 0$). These findings underscore the effectiveness of MIPs for environmental remediation of hazardous PAHs, such as fluorene. Future studies will focus on evaluating the selectivity of the synthesized MIP toward other PAHs and employ TGA to characterize the polymer further, particularly to assess template removal during the leaching process.

## ACKNOWLEDGEMENTS

This work was supported by Bandung Institute of Technology, Faculty of Mathematics and Natural Sciences, Department of Chemistry.

## REFERENCES

1. Lamichhane, S., Bal Krishna, K. C. and Sarukkalige, R. (2016) Polycyclic aromatic hydrocarbons (PAHs) removal by sorption: A review. *Chemosphere*, **148**, 336–353, Apr., 2016. doi: 10.1016/j.chemosphere.2016.01.036.

2. Idowu, O., Semple, K. T., Ramadass, K., O'Connor, W., Hansbro, P. and Thavamani, P. (2019) Beyond the obvious: Environmental health implications of polar polycyclic aromatic hydrocarbons. *Environ Int.*, **123**, 543–557, Feb., 2019. doi: 10.1016/j. envint.2018.12.051.

3. Mojiri, A., Zhou, J. L., Ohashi, A., Ozaki, N. and Kindaichi, T. (2019) Comprehensive review of polycyclic aromatic hydrocarbons in water sources, their effects and treatments. *Science of The Total Environment*, **696**, 133971, Dec., 2019. doi: 10.1016/j.scitotenv.2019.133971.

4. Honda, M. and Suzuki, N. (2020) Toxicities of Polycyclic Aromatic Hydrocarbons for Aquatic Animals. *Int. J. Environ Res. Public Health*, **17**, 4, 1363, Feb., 2020. doi: 10.3390/ijerph17041363.

5. Abdel-Shafy, H. I. and Mansour, M. S. M. (2016) A review on polycyclic aromatic hydrocarbons: Source, environmental impact, effect on human health and remediation. *Egyptian Journal of Petroleum*, **25**, 1, 107–123, Mar., 2016. doi: 10.1016/j.ejpe.2015.03.011.

6. Zhang, G., *et al.* (2018) The effects of different biochars on microbial quantity, microbial community shift, enzyme activity, and bio-degradation of polycyclic aromatic hydrocarbons in soil. *Geoderma*, **328**, 100–108, Oct., 2018. doi: 10.1016/j.geoderma.2018.05.009.

7. Noro, K. and Yabuki, Y. (2021) Photolysis of polycyclic aromatic hydrocarbons adsorbed on polyethylene microplastics. *Mar. Pollut. Bull*, **169**, 112561, Aug., 2021. doi: 10.1016/j. marpolbul. 2021.112561.

8. Liao, X., Zhao, D., Yan, X. and Huling, S. G. (2014) Identification of persulfate oxidation products of polycyclic aromatic hydrocarbon during remediation of contaminated soil. *J. Hazard Mater.*, **276**, 26–34, Jul., 2014. doi: 10.1016/j.jhazmat.2014.05.018.

9. Yogaswara, D. (2019) Adsorpsi Senyawa Polisiklik Aromatik Hidrokarbon (PAH) oleh Karbon Aktif. *Oseana*, **42**, 1, 1–8, 2019.

10. Bao, H., Wang, J., Zhang, H., Li, J., Li, H. and Wu, F. (2020) Effects of biochar and organic substrates on biodegradation of polycyclic aromatic hydrocarbons and microbial community structure in PAHs-contaminated soils. *J. Hazard Mater.*, **385**, Mar., 2020. doi: 10.1016/j.jhazmat. 2019.121595.

11. Song, X., *et al.* (2012) Determination of 16 polycyclic aromatic hydrocarbons in seawater using molecularly imprinted solid-phase extraction coupled with gas chromatography-mass spectrometry. *Talanta*, **99**, 75–82, Sep., 2012. doi: 10.1016/j.talanta.2012.04.065.

12. Ncube, S., *et al.* (2017) Synthesis and characterization of a molecularly imprinted polymer for the isolation of the 16 US-EPA priority polycyclic aromatic hydrocarbons (PAHs) in solution. *J. Environ. Manage*, **199**, 192–200, Sep., 2017. doi: 10.1016/j.jenvman.2017.05.041.

13. Yusof, N. A., Wei, W. L., Maamor, N. A. and Azeman, N. (2014) Preparation and characterization of molecular imprinted polymer for melamine based on methacrylamide and 9-vinylcarbazole as complexing monomer. *Asian Journal of Chemistry*, **26**, 8, 2285–2288. doi: 10.14233/ajchem.2014. 15699.

14. Zango, Z. U., *et al.* (2020) An overview and evaluation of highly porous adsorbent materials for polycyclic aromatic hydrocarbons and phenols removal from wastewater. *MDPI AG*, Oct. 01, 2020. doi: 10.3390/w12102921.

15. Feng Q., Chen Y., Xu D., Liu, L. and Zhang, Z. (2013) Molecularly Imprinted Micro-Solid-Phase Extraction for the Selective Determination of Phenolic Compounds in Environmental Water Samples with High Performance Liquid Chromatraphy. *Open Journal of Polymer Chemistry*, **03**, 03, 54–62. doi: 10.4236/ojpchem.2013.33011.

16. Noro, K. and Yabuki, Y. (2021) Photolysis of polycyclic aromatic hydrocarbons adsorbed on polyethylene microplastics. *Mar. Pollut. Bull*, **169**, Aug., 2021. doi: 10.1016/j.marpolbul.2021.112561.

17. Idowu, O., Semple, K. T., Ramadass, K., O'Connor, W., Hansbro, P. and Thavamani, P. (2019) Beyond the obvious: Environmental health implications of polar polycyclic aromatic hydrocarbons. *Elsevier Ltd.*, Feb. 01, 2019. doi: 10.1016/j.envint.2018.12.051.

18. Mojiri, A., Zhou, J. L., Ohashi, A., Ozaki, N. and Kindaichi, T. (2019) Comprehensive review of polycyclic aromatic hydrocarbons in water sources, their effects, and treatments. *Elsevier B.V.*, Dec. 15, 2019. doi: 10.1016/j.scitotenv.2019.133971.

19. Zhao, X., Pei, W., Guo, R. and Li, X. (2020) Selective Adsorption and Purification of the Acteoside in Cistanche tubulosa by Molecularly Imprinted Polymers. *Front Chem.*, **7**, Jan., 2020. doi: 10.3389/fchem.2019.00903.

20. Pinandita, A., et al. (2025) Anthrone-Based Dummy Molecularly Imprinted PVDF Membrane for Monitoring Fluorene and Phenanthrene in River Water. *Molecules*, **30(18)**, 3754, Sep., 2025. doi: 10.3390/molecules30183754.

21. Xin, L., Sun, H., Xu, R. and Yan, W. (2015) Origin of the structure-directing effect resulting in identical topological open-framework materials. *Sci. Rep.*, **5(1)**, 14940, Oct., 2015. doi: 10.1038/srep14940.

22. Krupadam, R. J., Ahuja, R. and Wate, S. R. (2007) Benzo(α)pyrene imprinted polyacrylate nano-surfaces: Adsorption and binding characteristics. *Sens Actuators B Chem.*, **124(2)**, 444–451, Jun., 2007. doi: 10.1016/j.snb.2007.01.020.

23. Sabrina, N., Ulianas, A., Yulkifli and Nurlely (2021) Molecularly Imprinted Polymer (MIPs) Nanomaterials Modified as Absorbing Cholesterol. *J. Phys. Conf. Ser.*, **1788(1)**, 012001, Feb., 2021. doi: 10.1088/1742-6596/1788/1/012001.

24. Hasanah, A. N., Safitri, N., Zulfa, A., Neli, N. and Rahayu, D. (2021) Factors Affecting Preparation of Molecularly Imprinted Polymer and Methods on Finding Template-Monomer Interaction as the Key of Selective Properties of the Materials. *Molecules*, **26(18)**, 5612. doi: 10.3390/molecules26185612.

25. Irawan, C., Dahlan, B. and Retno, 'N. (2015) Pengaruh Massa Adsorben, Lama Kontak dan Aktivasi Adsorben Menggunakan HCl Terhadap Efektivitas Penurunan Logam Berat (Fe) dengan Menggunakan Abu Layang sebagai Adsorben. *Jurnal Teknologi Terpadu*, **3**, 2.

26. Chen, X. (2015) Modeling of experimental adsorption isotherm data. *Information (Switzerland)*, **6(1)**, 14–22. doi: 10.3390/info6010014.

27. Krupadam, R. J., Korde, B. A., Ashokkumar, M. and Kolev, S. D. (2014) Novel molecularly imprinted polymeric microspheres for preconcentration and preservation of polycyclic aromatic hydrocarbons from environmental samples. *Anal Bioanal. Chem.*, **406(22)**, 5313–5321, Sep., 2014. doi: 10.1007/s00216-014-7952-z.

28. Ho, W. -L., Liu, Y. -Y. and Lin, T. -C. (2011) Development of Molecular Imprinted Polymer for Selective Adsorption of Benz[a]pyrene Among Airborne Polycyclic Aromatic Hydrocarbon Compounds. *Environ. Eng. Sci.*, **28(6)**, 421–434, Jun., 2011. doi: 10.1089/ees.2010.0268.

29. Krupadam, R. J., Khan, M. S. and Wate, S. R. (2010) Removal of probable human carcinogenic polycyclic aromatic hydrocarbons from contaminated water using molecularly imprinted polymer. *Water Res.*, **44(3)**, 681–688, Feb., 2010. doi: 10.1016/j.watres.2009.09.044.

30. Krupadam, R. J., Nesterov, E. E. and Spivak, D. A. (2014) Highly selective detection of oil spill polycyclic aromatic hydrocarbons using molecularly imprinted polymers for marine ecosystems. *J. Hazard Mater*, **274**, 1–7, Jun., 2014. doi: 10.1016/j.jhazmat.2014.03.050.

31. Nurwidiyani, R., Triawan, D. A. and Mawarti, S. (2025) Biobased Chitosan–Carbon Composite Beads from Azadirachta excelsa for Dual Dye Adsorption. doi: 10.21203/ rs.3. rs-7678806/v1.